Growth of diamond films on a diamond {001}(2×1):H surface by time dependent Monte Carlo simulations

E. J. Dawnkaski,[a] D. Srivastava, and B. J. Garrison
Department of Chemistry, The Pennsylvania State University, University Park, Pennsylvania 16802

(Received 4 October 1995; accepted 12 January 1996)

Time dependent Monte Carlo (TDMC) simulations are performed on a diamond lattice to determine the effect of surface properties/conditions on the growth of diamond thin films on flat and stepped diamond {001}(2×1):H surfaces under chemical vapor deposition conditions. The gas–surface interface consists of reactions of incoming gas-phase species, such as H_2 molecules and H and CH_3 radicals with surface radical, π-bond and step edge sites on the diamond {001}(2×1):H surface. The rates and probabilities of adsorption, abstraction, desorption, and incorporation reactions, as well as the reverse reactions, are explicitly calculated either via molecular dynamics or transition state theory methods, or taken from experimental measurements. The TDMC method allows all these reactions to occur simultaneously, though probabilistically, at each time step. The microscopic and macroscopic characteristics of the growing film are observed as functions of time. Diamond films of 10~100 layers are grown in the simulation and the observed growth rate (~0.5μm/h at 1200 K) is in agreement with experimental results. The contributions to the activation energy of growth by specific processes such as H abstraction, CH_3 adsorption and CH_2 incorporation into the trough sites have been determined. The contributions to the activation energies by specific processes are not linearly additive, and the CH_3 adsorption at step edges leads to enhanced growth at the edges.
© *1996 American Institute of Physics.* [S0021-9606(96)01915-X]

I. INTRODUCTION

In a recent investigation[1,2] we have implemented time-dependent Monte Carlo (TDMC) simulations for modeling diamond growth under chemical vapor deposition (CVD) conditions. Whereas typical Monte Carlo calculations are aimed at extracting equilibrium configurations, it is possible to add the time dimension and to estimate the characteristics of evolving quantities. For example, in our previous application of this method, a two-dimensional diamond {001}(2×1) surface in the presence of a gaseous environment of H atoms and H_2 molecules was considered. The quantities of interest were the concentration and distribution of radical sites. It is the radical sites onto which C containing species adsorb and consequently promote diamond growth. Processes such as H atom and H_2 molecule adsorption and desorption, H atom abstraction as well as H atom diffusion were included in these TDMC simulations. We were able to determine the equilibrium concentration of radical and π-bonded sites as a function of temperature. Moreover, we could determine the time related quantities such as lifetime of radicals and π bonds and the diffusion length of the radicals before they are destroyed either by adsorption of a gas phase species or by combination with other radicals to form π bonds.

The TDMC method[1,2] developed so far equates the Monte Carlo time step, δt, to the real time as measured experimentally in a simple and straightforward manner. Given a set of reaction rates, the probability of a specific reaction happening in any time step is expressed as the product of the rate and the time step. A constant time step for the simulation is chosen which is smaller than the duration of the fastest process considered. Thus the probabilities for the given set of all the reactions are between 0 and 1. During each time step all of the particles in the system are allowed to move albeit probabilistically. The reaction for an individual particle is chosen randomly and either allowed to occur or not based on its probability as defined above. In this manner the system dynamically evolves with time.

The goal of this work is to extend the TDMC method to be able to apply it to a real three dimensional growth. The necessary adaptations of the methodology are chosen in order to mimic the experimental conditions of CVD diamond growth. The diamond growth rate is dependent upon many factors which in essence determine the concentration of the reactants at the surface. The hot filament CVD growth of diamond typically occurs in a gaseous hydrogen environment at low total pressures of approximately ~20–30 Torr.[3–5] The major species in the gas phase are H_2, CH_4, C_2H_2, H, and CH_3, with the last two being considered as the important species for growth.[6,7] The experimental growth rates for hot filament CVD growth of diamond films are in the 0.1 to 1 μ/h range.[8–10] The apparent activation energy of the growth on diamond {001} is 8 kcal/mol.[11]

There are several challenges to overcome to extend and apply the TDMC prescription to realistic diamond growth in three dimensions. First, one must construct a diamond lattice for the simulation. Diamond does not follow the traditional solid-on-solid model. Rather it has four unique planes of atom positions as shown in Fig. 1. Moreover, on the {001} surface, C atoms pair up to form surface dimers, shown with a W–E orientation in Fig. 1. The surface dimers in the next layer, however, orient N–S. Thus reorientation introduces a

[a]Current address: Department of Chemistry, College of William and Mary, P.O. Box 8795, Williamsburg, VA 23185.

 0021-9606/96/104(15)/5997/12/$10.00 © 1996 American Institute of Physics

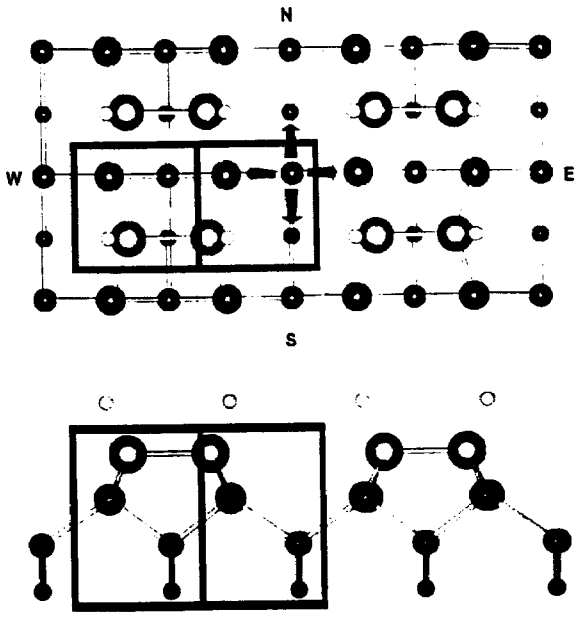

FIG. 1. A top and side view of a ball and stick model of the diamond{001}(2×1):H surface. Shown in both views are two rectangles which enclose atoms with the same horizontal (i,j) grid values (see the text). The H atoms are represented by the smallest and lightest spheres. The remainder of the spheres represent C atoms with the largest spheres corresponding to the surface atoms. The arrows in the top view point to the four carbon atoms (two above and two below) bonded to the third layer carbon atom. In the side view two H-terminated surface dimers are shown. If both H atoms are removed from one surface dimer a strained π-bond results.

logistical bookkeeping problem. Second, the list of possible reactions and events greatly increases as one must now include hydrocarbon species such as methyl, CH_3, radical. The CH_3 radical can adsorb onto and desorb from the surface, the H atoms of the CH_3 radical can also desorb, be abstracted or diffuse down onto a radical on the surface thereby leading to reactions on the surface that promote growth. Three-dimensional growth increases the number of different types of surface configurations even further as there are atoms at the step edges. Third, after the list of possible reactions is constructed, the rates for all the processes must be determined. It is possible that rates of key processes at the step edges are different from those on flat terraces. Finally, there is the issue of time scale. The growth rate is microns per hour, yet there are individual events such as the lifetimes of radicals that are on the order of microseconds. In the two-dimensional TDMC simulations we used MC time steps of $\sim 0.01-0.1$ μs. To grow even a few layers with this time step is very computationally intensive.

We have developed the methodology to perform a three-dimensional TDMC simulation of diamond film growth under CVD conditions. Various other researchers have developed kinetic MC[12–19] or TDMC[20–29] approaches. In this study we have increased the number and complexity of reaction events that are explicitly included. Of note are three of the kinetic MC studies of processes relating to diamond growth. Frenklach has modeled the concentration and distribution of radicals and diradicals on diamond[12] but has not included either the time domain or the energetics specific to π-bond sites. Frenklach also incorporated the tetrahedral diamond structure and adsorption of CH_3 and C_2H_2 onto an adamantane seed crystal.[13] He assumed that the surface reactions occur instantaneously. Consequently, the time in his simulation is related to the collision time of the various gas phase species. Finally, Xing and Scott have modeled acetylene adsorption, desorption and reaction with a diamond {111} surface.[16] They have based their MC moves on initial and final state energy differences which inherently assumes equilibrium at every step.

The TDMC simulations presented here predict a growth rate and Arrhenius activation energy in agreement with values observed experimentally.[11] In agreement with studies of Harris and Goodwin[30] we find that the CH_3 adsorption controls the overall growth rate. Additionally the method allows us to understand a microscopic picture of the events as they occur during the growth. The hydrogen abstraction reaction is shown to have the largest contribution towards the activation energy at temperatures approximately between 900 and 1200 K. A new CH_2 insertion mechanism in a trough between two dimer rows is identified as a rate limiting step at 800 K and below. The contributions to the overall activation energy by H abstraction, CH_3 concentration and trough insertion mechanism are not linearly additive. The concentration of the surface species at all times during the simulation as well as a snapshot of the growing surface are determined which provide further insight into the growth process.

In Sec. II we describe the model for the diamond lattice, the catalog of reactions included, the determination and values of the individual rates and reconciliation of time scales varying over many orders of magnitude. Section III discusses the TDMC method and the resulting growth rate and microscopic dynamics. In Sec. IV the main results of the general approach are summarized.

II. METHOD

A. The diamond lattice

The hydrogen terminated diamond {001}(2×1):H lattice is shown in Fig. 1. The diamond lattice (looking down at the {001} surface) repeats every four layers. Each bulk C atom in the lattice is fourfold coordinated and is bonded to two C atoms in the layer above and two C atoms in the layer below as shown for a third layer atom by the arrows in Fig. 1. In addition there is a layer dependent directionality. For example, the neighbor atoms above a third layer atom are in the W–E direction. For a second layer atom, however, the neighbor atoms in the layer above are in the N–S direction. In addition, the {001}(2×1):H surface consists of hydrogenated surface dimers which in Fig. 1 are oriented W–E. The layer underneath, however, has dimers oriented N–S. As diamond growth occurs the top surface layer remains dimerized whereas C atoms in the inner layers have bulk configurations. One straightforward approach in establishing a grid to represent this surface is to use a three dimensional simple cubic structure in which each diamond lattice site corresponds to an equivalent point on the grid. In this case the

model is only 1/4 full because each successive layer is offset from the layers directly above and below it by 1/4 of the diamond unit cell length. A more efficient grid is constructed by considering one of the rectilinear cells denoted in Fig. 1. If all the atoms in this cell are considered to have the same horizontal grid indices (i,j), but a different vertical index, (k), corresponding to the layer number, then all allowed values of the set (i,j,k) correspond to a C atom position. The surface reconstruction is simply a perturbation of the surface atom's equilibrium lattice position and is kept track of by an additional array index. A convenient advantage of this model is that only one grid site exists in the trough between any two dimers. This model thus implicitly includes the steric hindrance effect of not allowing CH_x $(x=0-3)$ species to exist concurrently on adjacent dimer atoms.

The addition of a third dimension (depth) to the simulation need not significantly increase the computational requirements beyond that of a two-dimensional simulation. Most of the grid sites which contain fourfold coordinated bulk carbon atoms or empty grid sites during each time step of the computation can be ignored. Only the active sites in the growing interface are monitored during the simulation. The number of active sites considered is only ~1.5 times the number of sites for the two-dimensional case of surface diffusion. Another advantage of maintaining only the dynamic list of active sites at which adsorption, abstraction, desorption, and incorporation reactions occur at each time is that the list automatically gets restructured at each step. In particular, the few adjacent sites that might have conflicting moves also get restructured as the dynamics progresses.

B. Surface reactions

In this study simulating the CVD growth process includes the reactions involving carbon containing species on the surface, whereas previously[1,2] we had considered only reactions involving H or H_2. A basic requirement in any Monte Carlo calculation is that a finite list of events must be chosen. We have tried to make the list as complete as possible with the conditions that the incoming gaseous C species is methyl radical, CH_3, and that all reactions involving C species lead to either a diamond structure or a dimerized surface state and that there are no possible graphitic or amorphous C configurations. Some of these reactions were intuitively determined *a priori* while others appeared in preliminary simulations and were thus added to the list for the final simulations.

The complete list of surface events should include adsorption, desorption, reaction, and diffusive events. As is discussed in Sec. II D, we have included a time filter that separates out the fast diffusive processes which are then ignored. Adsorption and desorption events are relatively straightforward[2] and are delineated in Table I as reactions a–d. Growing epitaxial diamond requires that the surface dimers break and C atoms insert into the surface dimers as well as into the trough positions between the two surface dimers. Possible pathways for these steps are shown in Fig. 2. The dimer insertion mechanism (reaction e) was proposed

TABLE I. Surface reactions.

	Surface reaction
a	Hydrogen adsorption onto a radical site
a′	H desorption (reverse of a)
b	Hydrogen abstraction
b′	H deposition from H_2 (reverse of b)
c	H_2 desorption
c′	Dissociative H_2 addition (reverse of c)
d	CH_3 adsorption
d′	CH_3 desorption (reverse of d)
e	Dimer insertion (see Fig. 2)
f	BCN mechanism (see Fig. 2)
g	Trough insertion (see Fig. 2)
h	Dimerization

following molecular dynamics simulations[31] as a two step process where the starting configuration is a surface dimer with a H atom adsorbed on one C atom and a CH_2 radical on the other C atom.[32] The surface dimer opens forming an ethylenic configuration and then the CH_2 inserts into the epitaxial position. A one-step mechanism with an energetically high three-center transition state has also been proposed for the same product.[33]

A mechanism for bridging the trough position with a C atom (reaction f) has been proposed by Harris based on model studies on bicyclo [3,3,1] nonane (BCN).[34] The mechanism is similar to that shown in the middle of Fig. 2. The two adjacent surface dimers have a C atom inserted into them. In the trough region there is a radical on one C atom and on the other C atom there is a CH_2 radical. This is an almost perfect configuration for bonding across the trough. There are a couple of additional assumptions in the BCN mechanism.[30] First the authors assume that surface dimers have formed in the next layer whereas we do not make this assumption. We believe this to be a minor difference. Second, they assume perfect alignment of dimer-trough pairs. Our preliminary simulations showed that this assumption is not valid, thus a second trough mechanism as shown in Fig. 2 is considered. The difference between the trough insertion mechanism shown here (reaction g) and the BCN mechanism is that a surface dimer must be broken (middle of the three surface dimers) for the growth to continue.

The formation of new surface dimers (reaction h) occurs after CH_2 groups have inserted into adjacent surface dimer or trough positions (not shown). There is steric hindrance[35] between the H atoms and thus the two CH_2 groups dimerize, desorbing a H_2 molecule in the process. This process can also occur with two CH groups inserted into adjacent surface dimer or trough positions but in this case no H_2 is desorbed. The configuration of an inserted CH group did not arise very frequently in the simulation but it is included for completeness.

Given these reaction events, a number of surface sites appear in the calculations. These have been categorized into 12 different generic configurations as shown in Fig. 3. For configurations 1–10 the specific site of interest is the rightmost atom or radical. The odd numbered configurations up to

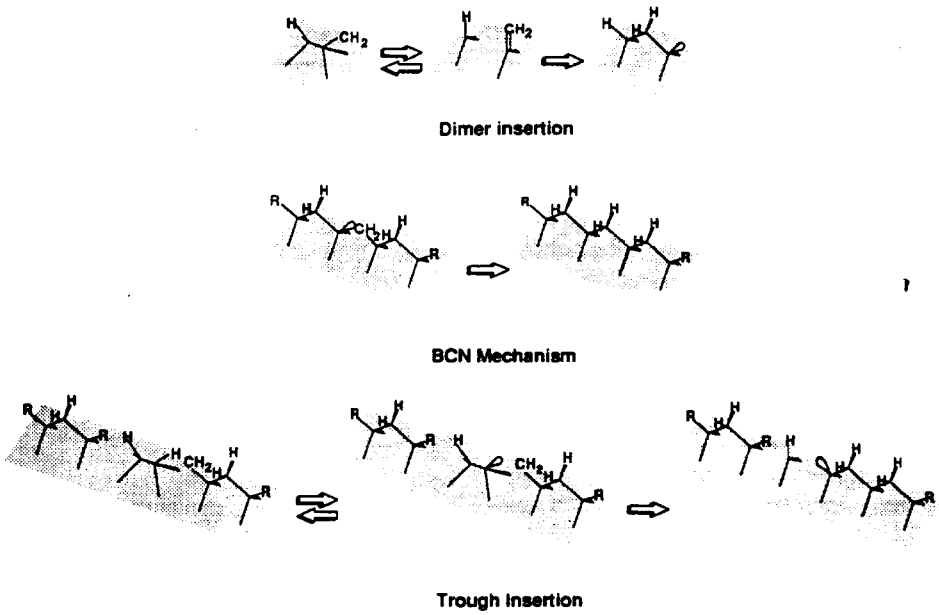

FIG. 2. The three types of insertion reactions considered for these simulations. They correspond from top to bottom to reaction types e, f, and g in Table I.

9 correspond to 2×1 dimer sites. The even number configurations up to 10 represent {111} sites. The {111} notation is used as the rightmost carbon atom has three C neighbors much like a C atom on the {111} surface. Configurations 11 and 12 represent epitaxial CH_2 and CH species, respectively. The reactions that can occur for each configuration are delineated in Table II. For example, in configuration 1, if the *R* group on the leftmost C is a radical, then at the radical on the rightmost C atom the following reactions can occur—H atom adsorption (reaction a from Table I), CH_3 adsorption (d), H atom deposition from H_2(b′), and dissociative H_2 adsorption (c′) since there are two radical sites on the same surface dimer, i.e., a π bond. On the other hand, if there is something else besides a radical on the leftmost carbon, then all of the above reactions can occur except the dissociative H_2 adsorption (c′). The computer code thus has approximately four times as many configurations as given in Fig. 3. Specifically, the configurations which differ only in the number of adsorbed H atoms are treated separately.

C. Rate constants and probabilities

Once the list of reactions has been determined, the rates for each must be evaluated. One of the key factors in being able to model such a complex growth process is being able to determine a rate for any required reaction. As with the previous investigation[1,2] we have taken the rates from a combination of molecular dynamics (MD) simulations, transition state theory (TST) and experimental values. For the MD simulations and TST calculations we have used the hydrocarbon potential developed by Brenner.[36,37]

For many of the individual reaction rates or energetics there are alternative calculated values in the literature. We have chosen to use a consistent set from the Brenner hydrocarbon potential. The results presented here of the TDMC calculation indicate that the trough mechanism is rate limiting at low temperatures. The energetics for this reaction have not been reported by others.

In this study we have used a temperature range of 800–1200 K since good quality diamond films are typically grown at temperatures less than 1300 K. For simplicity and lack of better information we have assumed that almost all the rates follow Arrhenius behavior, thus they can be described by an activation energy, E_a, and a frequency prefactor. The complete list of rates for each configuration of Fig. 3 is given in Table II. It is easier, however, to discuss them by type as given in Table I. More detail on how and why various approaches have been used is given in Ref. 2. The simple desorption events (a′ and d″) are assumed to have activation energies as defined by the bond strength using the Brenner

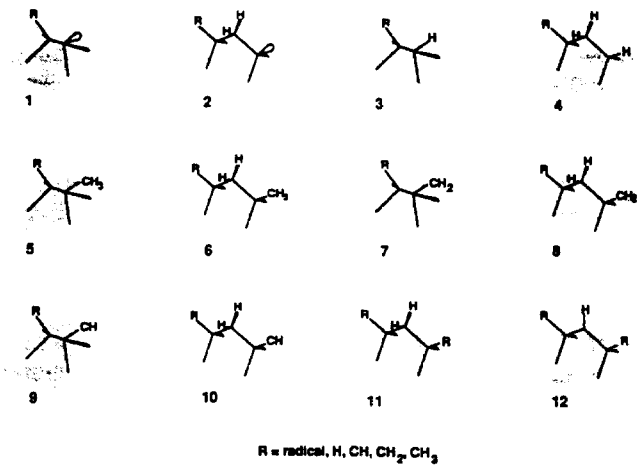

FIG. 3. The 12 basic surface configurations considered in the TDMC simulation.

TABLE II. Probabilities of reactions occurring at specific configurations as given in Fig. 3. The probabilities are given per $\delta t = 1\times10^{-5}$ s at 1200 K. For reactions involving gas phase species such as adsorption and abstraction, the probabilities were converted into their corresponding rates using the appropriate collision rate of (H, H_2, or CH_3) with the surface.[a] Partial pressures used for this table are 18 Torr for H_2, 0.1 Torr for H, and 0.01 Torr for CH_3.

Type	R^2	Reaction	Prefactor (s^{-1})	E_a (eV)	Probability	Ref.
1	Radical	a			5.11×10^{-1}	2
		d			6.50×10^{-4}	d
		b'	See note c	0.32	4.68×10^{-7}	2
		c'	See note b	1.25	1.92×10^{-10}	2
	H, CH, CH_2, CH_3	a			3.48×10^{-1}	2
		d			4.25×10^{-5}	d
		b'	See note b	1.25	2.65×10^{-3}	2
2	Any[c]	a			3.48×10^{-1}	2
		d			7.21×10^{-4}	42[d]
		b'	See note b	1.25	2.65×10^{-3}	2
3	Radical	b	8.7×10^{-1}	0.34	2.07×10^{-2}	2
		a'	1.0×10^{13}	3.43	3.93×10^{-7}	2
	H	c	1.0×10^{13}	3.14	6.49×10^{-6}	39
3,4	H, CH, CH_2, CH_3	b	1.3×10^{0}	0.42	1.47×10^{-2}	2
		a'	1.0×10^{13}	4.43	2.48×10^{-11}	2
5	Radical	d'	1.0×10^{13}	3.24	2.47×10^{-6}	d
5,6	Any	b	2.3×10^{0}	0.33	6.37×10^{-2}	2
		d'	1.0×10^{13}	4.24	1.56×10^{-10}	2
7,9	Any	e	See Table III and text			31,d
7,8	Any	b	8.7×10^{-1}	0.34	2.07×10^{-2}	d
7–10	Any	a			1.25×10^{-1}	d
8,10	Any	g	1.0×10^{13}	2.00	3.998×10^{-1}	d
	Any	f			1	d
11	Any	b	8.7×10^{-1}	0.34	2.07×10^{-2}	d
12	Any	a			3.48×10^{-1}	d
11,12	Any	h			1	d

[a]See P. W. Atkins, *Physical Chemistry*, 3rd ed. (Freeman, New York, 1986), p. 764 and Ref. 2.
[b]The functional group designated by R in Fig. 3.
[c]For the reverse reactions the activation energy is actually the energy difference between the initial and final configurations as discussed in Ref. 2.
[d]Rate constants determined in this work.
[e]"Any" refers to a radical, H, CH, CH_2, or CH_3.

potential. The prefactors are assumed to be 10^{13} s^{-1}. Care is taken to distinguish between final states of a single radical on a surface dimer and in a π bond as the energetics are different.

Hydrogen adsorption (a) and hydrogen abstraction (b) reactions were previously modeled by MD simulations for radical sites at temperatures between 1200 and 1800 K.[2] The abstraction values were fit to an Arrhenius form and extrapolated to temperatures lower than 1200 K. On the other hand, there is minimal temperature dependence in the adsorption probabilities as it is an unactivated process, thus the adsorption values calculated for 1200 K are also used at the lower temperatures. For comparison purposes the values of the H adsorption probability per site at 1200 K is 53% on a 2×1 radical site and 78% on a π-bond site. The H abstraction probability per site at 1200 K is ~2% for a 2×1 configuration that results in a radical and ~3% when it results in a π bond. For other configurations where H adsorption can occur to a radical on a lattice site, we chose to use the same value as that for adsorption at a radical site (53%). Exceptions to this are configurations 7–10 where more flexible CH_2 or CH adspecies are present. We performed MD simulations[38] at 1200 K and calculated a probability of 19% for H adsorbing to CH_2 to form CH_3. The adsorption probability on CH_2 group is lower than on a radical because the CH_2 group has more thermal motion than a radical attached to a lattice site. A value of 19% for the H adsorption probability is used for configurations 7–10.

We calculated H abstraction probabilities from a CH_3 adspecies and obtained probabilities of 9.4% at 1200 K, 19.3% at 1500 K, and 26.7% at 1800 K. The values on a per H atom basis are consistent with the values of 2%–3% for H atom on the surface at 1200 K.[2] Simulations were also performed for H abstraction from CH_2. The probability determined is 4.5% at 1200 K. At higher temperatures the CH_2 species inserted into the dimer (reaction e) thus abstraction calculations could not be performed. Since the 1200 K abstraction probability from a CH_2 adspecies is similar to that from a H saturated (2×1) surface, the previously determined values are used at all temperatures.

The MD studies of CH_3 adsorption were performed analogously to the H adsorption simulations. The gas phase CH_3 was equilibrated to the desired temperature before adsorption on the surface. For temperatures of 1200, 1500, and

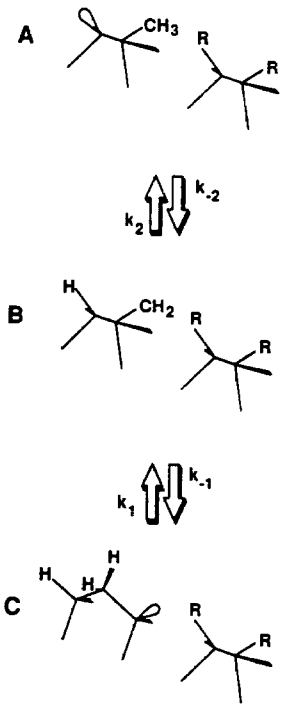

FIG. 4. A possible pathway for CH_2 insertion into the dimer bond starting with a CH_3 adsorbed on a dimer with a radical on the adjacent dimer atom. The values for the rate constants are given in Table III.

1800 K, the adsorption probabilities per site on a π bond are 3.82%, 3.9%, and 4.5% and on a radical site are 0.25%, 0.42%, and 0.33%, respectively. Given the statistical uncertainties, each set of numbers are indistinguishable from each other. We thus used the values of 3.82% and 0.25% for the two types of sites at all temperatures.

The H_2 desorption (c) probability was taken from experimental values.[39] The only mechanistic assumption made about the process is that the two hydrogen atoms must desorb from the same dimer on the surface. As discussed in Ref. 2 the reverse reaction rates of H atom deposition from H_2 (b′), and dissociative adsorption of H_2 (c′) are estimated from relative energetics. The values of the energy difference are given in Table I.

Reactions e and g which involve CH_2 insertion into a surface dimer or trough are shown in detail in Fig. 2. The activation energies and prefactors for these reactions have been calculated via a steepest descent path method[40] and a simple transition state theory[21] is used for the reaction rates as described previously.[2] The rates for any additional CH_x ($x=1-3$) reaction probabilities such as H transfer from a CH_3 to an adjoining radical (Fig. 4) have been calculated in a similar manner and are given in Table III. Reaction f, the BCN mechanism, is assumed to occur instantaneously with unit probability.

There are surface dimerization reactions (h) between either a pair of adjacent inserted CH_2 groups or CH groups. We have assumed that this is a highly favorable reaction and that the reactions occur instantaneously with unit probability.

TABLE III. Rate constants for equilibrium processes (as given in Fig. 4) which lead to the insertion of a CH_2 species into the dimer bond. Activation energies and prefactors are determined via SDP and TST calculations (see the text).

Rate constant	Prefactor [1]	Activation energy (eV)
k_1	$1.9\times$	1.51
k_1	$1.9\times$	1.21
k_2	$1.0\times$	1.65
k_2	$1.0\times$	1.28

The simulation conditions for gas–surface interface have been chosen for the concentrations of gas phase reacting species to match experimental conditions.[8–10] The simulations have been done at partial pressures for H atom, H_2 molecule and CH_3 radical set at 0.1, 18, and 0.01 Torr, respectively. These pressures are used to calculate[2] the reaction probabilities given in Table II. Corat and Goodwin[41] have reported that the CH_3 concentration decreases with temperature below approximately 1000 K. This decrease in CH_3 concentration which corresponds to an activation energy of ~4 kcal/mol has been taken into account in these simulations unless it is explicitly stated otherwise.

To summarize, all reaction probabilities at 1200 K are given in Table II. For activated processes the activation energy and prefactor are also given so that values at lower temperatures can be obtained. For reactions involving collisions with a gas phase particle, a collision factor which is temperature and partial pressure dependent has been used. The partial pressures used for Table II are given therein. Finally, as mentioned in the previous paragraph, an additional temperature dependence in CH_3 concentration has been used in the simulations unless stated otherwise.

D. Time scales

The discussion of the reconciliation of the overall simulation time duration with the lifetimes of the individual events is now in order. In the ideal case every possible reaction should be included in the MC calculation. Such a simulation cannot be completed on today's computers because there are many orders of magnitude difference between the fastest and the slowest reactions. We have partitioned the fast processes into two groups. The first group includes many of the surface processes that are either rare events that do not contribute significantly to the growth process or are those which lead to no net change in the system. For an in depth look into the atomistic details these events should be included, but can be dealt with in a different manner than the simulation of macroscopic quantities such as the film growth rate. For example, radical site diffusion on the surface has a lifetime of approximately 1 μs.[1,2] This lifetime is too small for diffusion to be monitored for a simulation that may last up to 40 s. Additionally, in our previous study[1,2] we have shown that, at temperatures below 1200 K, H atoms do not diffuse significantly during the lifetime of a radical site. Thus the H diffusion events can be ignored in a long time scale simulation of the growth. The second category of fast events

is exemplified by CH_2 insertion into a dimer bond. The CH_2 insertion event has a lifetime on the order of 10^{-8} s and is one of the primary mechanisms by which carbon is incorporated into the diamond lattice. Since a methyl radical collides with a surface site every 5×10^{-4}s the insertion reaction generally achieves equilibrium long before the next adsorption event occurs. One pathway for the insertion reaction, starting with an adsorbed methyl radical on a (2×1) dimer, is shown in Fig. 4. The corresponding prefactors and activation energies for the Arrhenius rate constants are given in Table III. One could take these rate constants, determine the equilibrium populations and then probablistically determine which configurations exist at any given time. An examination of the rate constants for the steps involved in the insertion reaction shows that at equilibrium the reaction has gone essentially to completion. Additionally the adsorption of any species onto the radical site in Fig. 4(c) will ensure that the reverse reaction does not occur. Thus the insertion reaction is treated as irreversible.

In summary, the timescales of the fastest and slowest processes in this work differ by many orders of magnitude. There are two possible approaches to including both kinds of processes in a single simulation. First, the simulation is performed in time steps suitable to the fast processes and very slow processes are incorporated as rare events through appropriate schemes.[1,2] Second, the simulation is performed in time steps suitable for rate determining slow processes and the fast processes are included as though at each time step all the fast processes have achieved chemical equilibrium. We choose the second approach because the focus is on the overall growth rates with the microscopic dynamics of fast processes also included.

E. TDMC calculation

Given an ensemble of microscopic reactions in a system, the essence of the time dependent Monte Carlo calculation is how the system evolves towards the equilibrium configuration. A template or grid of sites is established on which the individual reactions occur. The sites are cycled through, and from a Monte Carlo approach various events are allowed to proceed. Since we are considering a multitude of competing processes for many particles simultaneously, an important consideration is the method by which we extend the Monte Carlo calculation into the time domain. Our method is based upon the observation that given the rate of each individual process in a system, the probability of a process occurring within any specified time period or time step is simply the product of the time step and the rate for the process. A single constant time step, δt, for the overall dynamics is chosen such that it is greater than the duration of the fastest process considered. The probabilities for all of the considered processes are thus between 0 and 1. All of the particles are allowed to move in each step with the process for each particle randomly selected. A particle moves, however, only if the probability of the move is less than a uniformly sampled random number between 0 and 1. The constant time step is chosen such that the acceptance probability of the fastest process is about 0.5, a value typical of most MC simulations. In this procedure a value of $\delta t=10^{-5}$ is chosen. A comparative discussion of different TDMC methods is given in Ref. 2.

We are interested in the dynamics on a diamond {001}(2×1) surface with the goal of growing a few layers of diamond. For a flat {001}(2×1) surface the grid chosen is 10×10 points, with periodic boundary conditions, in which each grid point is a surface C atom. The TDMC calculation proceeds by keeping track of all the grid points at the interface. In a single time step all grid points are checked for the possibility of adsorption, desorption, abstraction, or reaction events. The growth rate as well as surface structure are monitored at each time step. The model allows the determination of the surface concentration of all species and the overall activation energy. The contributions to the activation energy from specific events can also be calculated.

III. RESULTS AND DISCUSSION

The TDMC simulations are carried out to study (i) the overall growth rates and comparison to experiments, (ii) the activation energy for growth and factors contributing to it, and (iii) the growth on a stepped {001}(2×1):H surface. Since CH_3 adsorption is the source for depositing and subsequently incorporating C in the growing diamond lattice, the growth rates are determined for a series of simulations, each having different CH_3 adsorption behavior on a flat diamond (2×1):H surface. These simulations are discussed and compared with experiments in Sec. III A. The contributions to the overall activation energy of growth by different gas–surface reactions such H abstraction, CH_3 insertion into trough sites and gas phase CH_3 concentration are explored in Sec. III B. In Sec. III C we report simulations on a single stepped diamond {001}(2×1):H surface and monitor the time development of the various types of reactions and the sites on the surface.

A. Growth rates and CH_3 adsorption probabilities

Since the adsorption of CH_3 is the major means of adding carbon to the surface and helps to govern the growth rate we have chosen three different CH_3 adsorption schemes. In the first scheme the adsorption probability for CH_3 is the same for all the surface sites and is set to the value (6.5×10^{-4} at 1200 K or 3.82%) calculated for adsorption onto configuration 1, reaction d (R=radical, i.e., a π bond) as given in Table II. In the second scheme the CH_3 adsorption probability on a terrace site is set to the value (4.25×10^{-5} or 0.25%) calculated for adsorption onto the configuration 1, reaction d (R=nonradical) and the π bond adsorption probability remains unchanged at 6.5×10^{-4}. In the third scheme different configurations have different CH_3 adsorption probabilities. The reaction probability at an isolated radical on a terrace is given in Table II, as reaction d under configuration 1 when R is a nonradical (4.25×10^{-5}). Adsorption at a π bond is given by the value for site configuration 1 and reaction d when R is a radical site (6.5×10^{-4} at 1200 K). Finally adsorption at a step is given

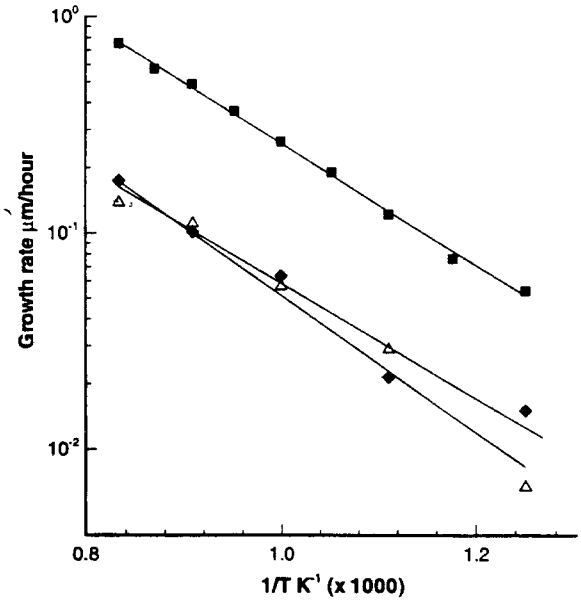

FIG. 5. Plot of the log of the diamond growth rate vs inverse temperature. Data for the three schemes explained in the text are shown. The solid squares correspond to scheme 1, the open triangles to scheme 2, and the solid diamonds to scheme 3.

by the {111} step edge adsorption probability (4.24%) as calculated by Perry and Raff using the same interaction potential as we have used in this work.[42] The step probability is assigned if any site adjacent to the radical site being considered is vacant, or if two radical sites are adjacent to one another in a configuration other than a π bond.

In Fig. 5 the growth rate is plotted versus the inverse temperature for the three simulation schemes. The lower growth rates are observed for schemes 2 and 3 where the CH_3 adsorption probabilities on a terrace site are lower, but more realistic, than in scheme 1. The growth rates in both the cases are similar to those reported by Chu *et al.*[11] for homoepitaxial growth on the diamond {001} surface where the observed growth rate changes from approximately 0.08 μ/h at 1000 K to 0.5–0.9 μ/h at 1250 K. The variation in the overall magnitude of the growth rate seen by changing the CH_3 adsorption probability supports the supposition that the adsorption of CH_3 is one of the rate determining steps in the film growth.[30] In all the three cases we see that the growth rates follow Arrhenius behavior.

B. Activation energy of growth

The Arrhenius activation energy of the overall growth process can be calculated directly from the growth rate data in Fig. 5. Experimentally, Kondoh *et al.*[43] have reported an activation energy of 22–24 kcal/mol for polycrystalline diamond growth on a Si{001} substrate and Chu *et al.*[11] have reported an activation energy of 8 kcal/mol for homoepitaxial diamond growth on the {001} surface. We have calculated an activation energy of 12.9 kcal/mol where the CH_3 adsorption probabilities are all the same (scheme 1), 12.2 kcal/mol for the second scheme and 14.5 kcal/mol for the

TABLE IV. Arrhenius activation energies of growth for TDMC simulations which include different temperature dependencies.

Case	H abstraction	CH_3 concentration	Trough insertion	E_a (kcal/mol)
1	×	×	×	12.9
2	×		×	10.5
3	×	×		11.9
4	×			8.1
5		×		2.7
6			×	NA
7				−0.1

case where the CH_3 adsorption probabilities differ by local configurations. The contribution to the activation energy by different CH_3 adsorption probabilities is about 10%. The predicted activation energies are within the range of the experimental values. It is important to note that the input to the TDMC calculations has come from individual reaction rates and that no fitting of the overall growth rate to the experimental data has been performed.

It is not obvious from the energetics given in Table II which of the reactions controls the activation energy of the overall growth process. To delineate which process dominates, we considered the temperature dependence of the H abstraction process (radical creation), the gas phase CH_3 concentration, and the trough insertion reaction (g). By selectively keeping constant the temperature dependence of one or more of these processes, we can determine the effect of the specific process on the activation energy. Listed in Table IV are the temperature dependences that are included for each of the different simulations plotted in Fig. 6. Case 1 of Table IV and Fig. 6 is the same as scheme 1 of Fig. 5 and includes all temperature dependences. Before discussing the

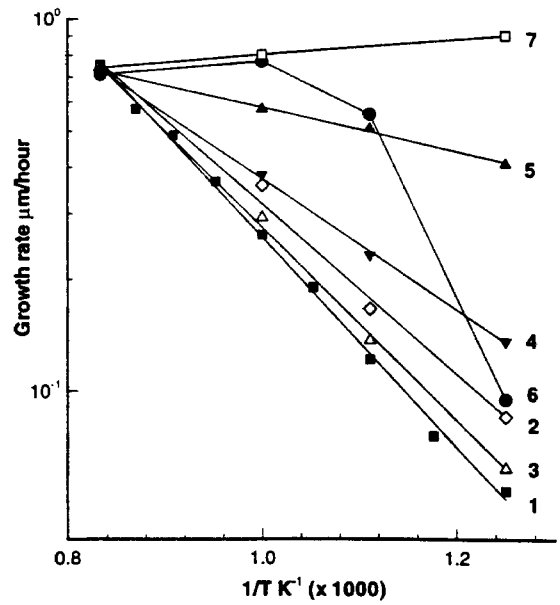

FIG. 6. Plot of the log of the diamond growth rate vs inverse temperature. The seven curves correspond to the seven different cases of temperature dependencies listed in Table IV.

specific calculations there are two factors to mention. First, hidden in the temperature dependence of the H abstraction probability and the gas phase CH_3 concentration is the temperature dependence of the collision frequency[2] with the surface which is proportional to $1/\sqrt{T}$. This factor has a negligible effect on the activation energy as evidenced by the results of case 7 where only the collision frequency is altered with temperature. Therefore, the temperature dependence of the collision frequency is included in all the calculations even though it is not explicitly mentioned. Second, if a quantity is held constant with temperature, the value at 1200 K is used, thus all the curves in Fig. 6 converge at 1200 K.

The first striking conclusion reached from the results in Table IV and Fig. 6 is that omitting any of the temperature dependences reduces the activation energy. A closer examination shows that the largest contribution (8–9 kcal/mol) to the overall activation energy is due to H abstraction (case 4) and this contribution is consistent with activation barriers calculated for the abstraction reactions. The contributions from all the three processes are also not linearly additive. For instance, the value of E_a in case 5, where only the T dependence of the CH_3 concentration is retained, is 2.7 kcal/mol which if added to that for case 4 gives 10.8 kcal/mol. On the other hand, case 3 exhibits an activation energy of 11.9 kcal. Additionally the contribution from the trough insertion reaction (case 6) is clearly not linear. The CH_3 concentration and the trough insertion process are strongly coupled to each other. The trough insertion process appears to be the rate limiting step at low temperatures as evidenced by the large decrease in observed growth rate at 800 K in case 6. This is confirmed by looking at a snapshot (Fig. 7) of the growing surface at 800 K with all the temperature dependencies included. After 0.5 s the surface has started to grow and several pits are apparent on the surface. In the next 3.0 s all but one of the pits has filled in and the surface continues to grow around the pit at the left edge of the surface in the lower half. Part of the same pit is also seen at the right edge because of the periodic boundary conditions. The configuration in the pit is the same as the initial condition for the trough insertion reaction shown in Fig. 2. Growth at 10.0 s has stopped and cannot continue until the trough insertion takes place.

In summary, the H abstraction process dictates the activation energy for temperatures approaching 1200 K. At the lowest temperature investigated (800 K), however, the trough insertion mechanism is the rate limiting step. It is, in fact, the observation in the simulation of bottlenecks such as that shown in Fig. 7 that forced us to include the trough insertion mechanism in addition to the Harris's BCN mechanism. This simulation thus points out the need to use a higher level of electronic structure calculations to determine a more accurate estimate of the activation energy for trough insertion of a CH_x species.

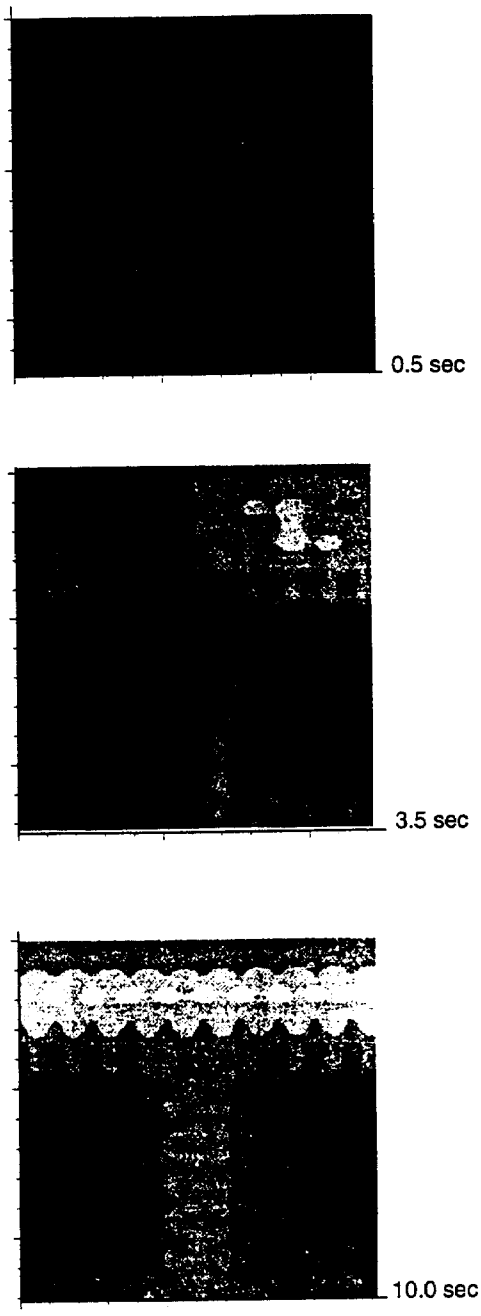

FIG. 7. Three topographical snapshots of a growing diamond surface for case 1 at 800 K with snapshots at 0.5, 3.5, and 10 s. The surface area shown is a square of side 25 Å and the plot is shaded by layer number with the highest layer being the lightest in shade. The surface of the original crystal is black and initially lower layers can also be seen as it is possible to see four layers deep into the diamond crystal. This sequence shows the growth being halted at 16 layers in 10 s while waiting for a trough insertion event to occur in the pit at the left edge in the lower half.

C. Effect of surface steps

In order to gain better insight into the processes affecting the growth rate and activation energy, the calculations discussed in Sec. III A have been repeated at 1200 K for a larger grid size and with a stepped surface using the same three CH_3 adsorption schemes as described above. The initial configuration of the 20×20 grid is shown in Fig. 8. The dimer rows on the terraces can clearly be seen with individual dimer atoms represented by ovals. From the initial configuration the simulation proceeded for 10 s. During the course of the growth the number densities of all the surface species were collected. The results for schemes 2 and 3 are quanti-

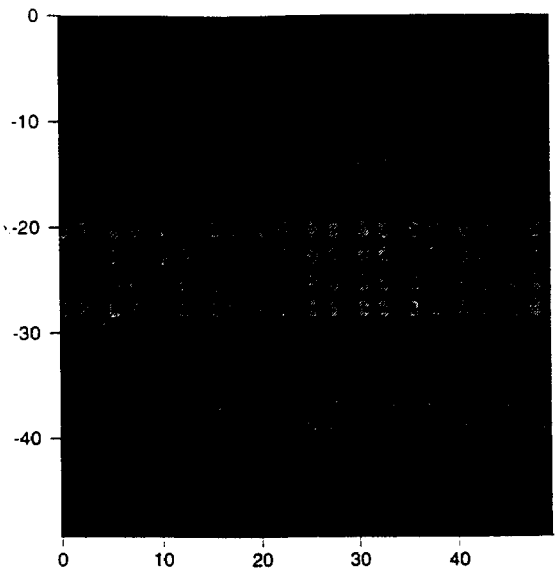

FIG. 8. The initial surface configuration for the stepped surface studies. The dimer rows on each terrace are rows of adjacent ovals. The axis scale is in angstroms and the plot is shaded similarly to Fig. 7.

tatively and qualitatively similar so only data for schemes 1 and 3 are shown in Figs. 9(a) and 9(b). The primary differences between schemes 1 and 3 are the number of dimer sites (configuration 3 in Fig. 2) and the number of {111} CH_x ($x=1-3$) configurations (sum of configurations 6, 8, and 10 in Fig. 2). For scheme 1 approximately 20% of the surface sites are dimers at any given time indicating a continued presence of sites which allow for quick incorporation of carbon into the lattice via the dimer insertion mechanism of Fig. 2. Additionally this implies that only a small number of surface CH_x species are waiting to be incorporated into the lattice via the other two trough insertion processes. Conversely the dimer sites in scheme 3 are quickly consumed and the surface {111} CH_x ($x=1, 3$) species are left waiting for an incorporation pathway. This is primarily due to an order of magnitude decrease in the CH_3 adsorption probability on the terraces and at other sterically hindered sites. Since diffusion is not considered in this simulation, it is necessary for two CH_3's to adsorb next to each other to form a new dimer bond in the next layer. In the case of scheme 1 such event happens with regularity whereas in schemes 2 and 3 it becomes less frequent because CH_3 adsorption probability is low. In the latter case as soon as a newly formed dimer loses a hydrogen it reacts with another gas phase species to form {111} CH_x type of site. The increased abundance of CH_x sites in scheme 3 leads to a slower growing and rougher surface.

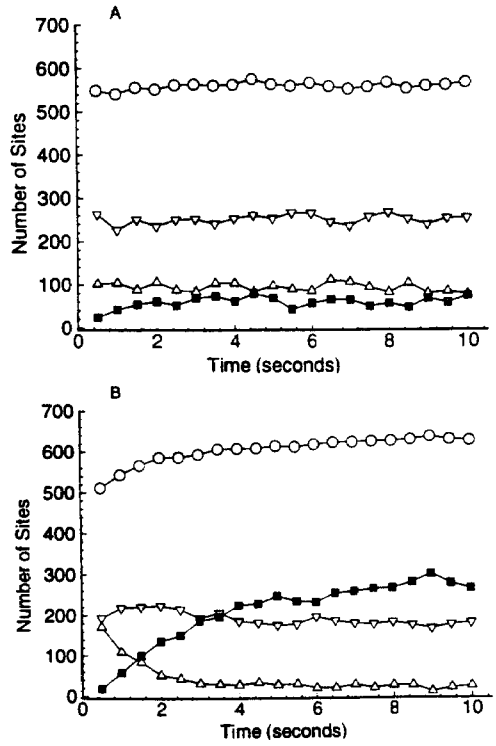

FIG. 9. A comparison of the number density of the different surface species for schemes 1 and 3 as a function of time for the stepped surface. Scheme 1 and 3 are represented by graph A and B, respectively. ○—sum of all sites of type 1–12, ▽—type 4, △—type 3, ■—sum of types 6, 8, and 10.

In terms of the actual surface configuration, the expectation thus would be for scheme 3 to show growth along step edges and that there should be some retention of surface features due to the higher reactivity at step edges. Conversely in scheme 1 one would expect a quickly growing smooth surface devoid of surface features. Figures 10(a) and 10(b) show the growing diamond surface at 0.5, 3.5, and 10.0 s for schemes 1 and 3, respectively. As expected, scheme 1 shows a fast growing smooth surface with the completion of almost 25 layers within the 10 s simulation. The scheme 3 on the other hand, exhibit slower and rougher growth of only eight layers in a 10 s simulation. The most prominent surface hydrocarbon species is the epitaxial CH_2 species which have inserted into the dimer or trough. These CH_2 species tend to grow in rows perpendicular to the dimer rows on the surface and can be seen as individual lines of approximately 2 Å in width in Fig. 10(a). When two of these lines appear next to each other they indicate the formation of dimers on the surface. Individual carbon centers are seen as ovals and no distinction can be seen among any of the CH_x species. Scheme 3 [Fig. 10(b)] shows a rougher and slower growing surface with some retention of surface features. Initially the addition of CH_3 species occurs at the step edges and similar to scheme 1 we see rows of CH_2 form perpendicular to the dimer rows. By 3.5 s most of the easily accessible sites have been filled and the growth must now wait for the deeper and hindered sites to be filled. It is at this point that we see a change in the growth rate that reflects a dependence on the lower CH_3 adsorption probability at the hindered site.

Although scheme 3 represents a more realistic physical picture of diamond growth, the growth rate is lower than that seen experimentally and the topographical picture of the surface does not show the rows of dimers that are observed in scheme 1 and in STM pictures of the diamond{001} surface after growth.[44] One reconciliation of this difference might be the inclusion in the simulation of surface diffusion processes

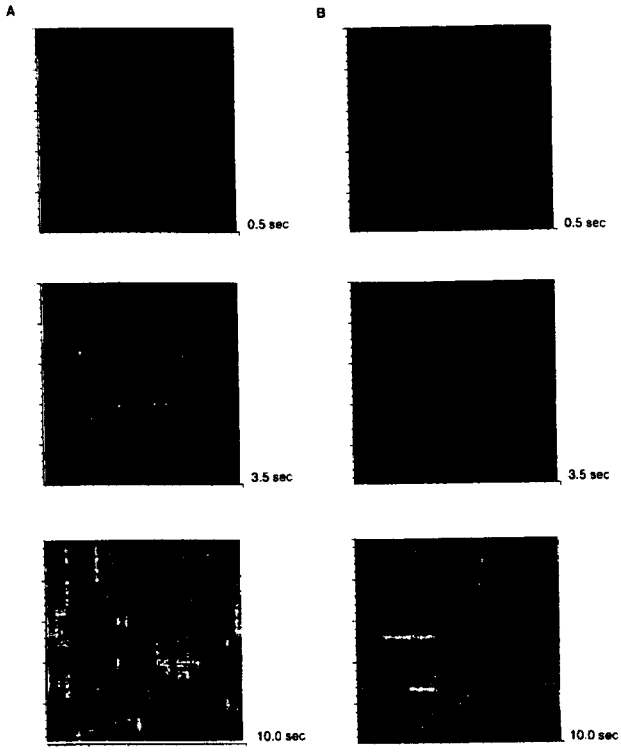

FIG. 10. Snapshots taken at 0.5, 3.5, and 10 s of diamond surfaces grown on the substrate shown in Fig. 8, under schemes 1 (A) and 3 (B). The plots are shaded similarly to figures 7 and 8. At 0.5 s both the schemes show growth of 8 layers. At 3.5 s scheme 1 in (A) shows smoother growth of 12 layers while scheme 3 in (B) still shows only 8 layers with many pits in the growing interface. The final growth at 10 s is of 25 layers in (A) and of 8 layers in (B).

involving CH_x species. One specific diffusion process that may lead to surfaces which look more like the STM imaged surfaces would be the diffusion of CH_2 along the dimer rows. A CH_2 could diffuse along a dimer row until it collides with another CH_2 species and then dimerizes. This would serve the purpose of converting CH_2 species into dimer species resulting in rows of dimers on the surface rather the rows of CH_2's presently observed. Another important process may be diffusion of C containing species along the step edges or interlayer diffusion.[45] It may be easier for a C to be incorporated into the lattice at sites with low adsorption probabilities if the carbon species can diffuse to that site. This could serve to both lower the activation barrier and increase the growth rate.

IV. CONCLUSIONS

A TDMC simulation of hot filament CVD diamond growth has been presented which qualitatively matches the results of experimental growth studies. Both the growth rate and the activation energy are similar to those experimentally observed for homoepitaxial diamond growth on diamond{001} surfaces. The growth is seen to be limited by the adsorption of CH_3 at sterically hindered reaction sites and by the trough insertion at low temperatures. On a stepped surface the growth occurs mainly at the step edges as expected. It is likely that the difference between these results and experiment may be due to surface diffusion processes that have not been considered in this simulation. Nonetheless separate domains on successive layers have been observed which are similar to those seen in the STM images. Not only have the macroscopic quantities such as the growth rate been determined but the concentrations of the surface species at any time during the simulation has also been extracted to yield useful microscopic information about the growth process under different reaction conditions.

ACKNOWLEDGMENTS

We gratefully acknowledge financial support from the Office of Naval Research. We thank Professor Ken S. Feldman for insightful conversations on organic chemistry and diamond film growth processes. The computational support for this work was provided by the IBM-SUR program at the Penn State University.

[1] E. J. Dawnkaski, D. Srivastava, and B. J. Garrison, Chem. Phys. Lett. **232**, 524 (1995).
[2] E. J. Dawnkaski, D. Srivastava, and B. J. Garrison, J. Chem. Phys. **102**, 9401 (1995).
[3] F. G. Celii, P. E. Pehrrson, H.-T. Wang, and J. E. Butler, Appl. Phys. Lett. **52**, 2043 (1988).
[4] F. G. Celii and J. E. Butler, Appl. Phys. Lett. **54**, 1031 (1989).
[5] S. J. Harris, A. M. Weiner, and T. A. Perry, Appl. Phys. Lett. **53**, 1605 (1988).
[6] See, for example, R. Haubner and B. Lux, Diamond and Related Materials **2**, 1277 (1993); C.-P. Klages, Appl. Phys. A **56**, 513 (1993); J. C. Angus, A. Argoitia, R. Gat, Z. Li, M. Sunkara, L. Wang, and Y. Wang, Philos. Trans. R. Soc. London, Ser. A **342**, 195 (1993).
[7] See, for example, J. E. Butler and R. L. Woodin, Philos. Trans. R. Soc. London, Ser. A **342**, 209 (1993), and references therein.
[8] W. L. Hsu, Appl. Phys. Lett. **59**, 1427 (1991).
[9] S. J. Harris and A. M. Weiner, J. Appl. Phys. **67**, 6520 (1990).
[10] F. G. Celii and J. E. Butler, J. Appl. Phys. **71**, 2877 (1992).
[11] C. J. Chu, R. H. Hauge, J. L. Margrave, and M. P. D'Evelyn, Appl. Phys. Lett. **61**, 1393 (1992).
[12] M. Frenklach, Phys. Rev. B **45**, 9455 (1992).
[13] M. Frenklach, J. Chem. Phys. **97**, 5794 (1992).
[14] P. W. Rooney and F. Hellman, Phys. Rev. B **48**, 3079 (1993).
[15] Z. Zhang and H. Metiu, Surf. Sci. Lett. **292**, L781 (1993).
[16] J. Xing and H. L. Scott, Phys. Rev. B **48**, 4806 (1993).
[17] S. Pal and D. P. Landau, Phys. Rev. B **49**, 10597 (1994).
[18] J. M. McCoy and J. P. LaFemina, Phys. Rev. B **50**, 17127 (1994).
[19] J. Cortes, E. Valencia, and P. Araya, J. Chem. Phys. **100**, 7672 (1994).
[20] D. T. Gillespie, J. Phys. Chem. **81**, 2340 (1977).
[21] A. F. Voter, Phys. Rev. B **34**, 6819 (1986).
[22] H. C. Kang and W. H. Weinberg, J. Chem. Phys. **90**, 2824 (1989).
[23] L. A. Ray and R. C. Baetzold, J. Chem. Phys. **93**, 2871 (1990).
[24] A. M. Bowler and E. S. Hood, J. Chem. Phys. **94**, 5162 (1991).
[25] D. Srivastava and B. J. Garrison, J. Chem. Phys. **95**, 6885 (1991).
[26] K. A. Fichthorn and W. H. Weinberg, J. Chem. Phys. **95**, 1090 (1991).
[27] D. Srivastava and B. J. Garrison, Phys. Rev. B **46**, 1472 (1992).
[28] D. Srivastava and B. J. Garrison, Phys. Rev. B **47**, 4464 (1993).
[29] P. L. Cao, Phys. Rev. Lett. **73**, 2595 (1994).
[30] S. J. Harris and D. G. Goodwin, J. Phys. Chem. **97**, 23 (1993).
[31] B. J. Garrison, E. J. Dawnkaski, D. Srivastava, and D. W. Brenner, Science **255**, 835 (1992).
[32] As discussed in Refs. 1 and 2, there are several routes to achieving this configuration including adsorption of a CH_3 radical onto a surface π bond and then migration of one H atom from the adsorbed CH_3 to the adjacent radical.
[33] D. Huang and M. Frenklach, J. Phys. Chem. **96**, 1868 (1992).
[34] S. J. Harris, Appl. Phys. Lett. **56**, 2298 (1990).
[35] Y. L. Yang and M. P. D'Evelyn, J. Vac. Sci. Technol. A **10**, 978 (1992).

[36]D. W. Brenner, Phys. Rev. B **42**, 9458 (1990).
[37]D. W. Brenner, J. A. Harrison, C. T. White, and R. J. Colton, Thin Solid Films **206**, 220 (1991).
[38]For all simulations reported here a total of 2400 trajectories were calculated.
[39]R. E. Thomas, R. A. Rudder, and R. J. Markunas, J. Vac. Sci. Technol. A **10**, 2451 (1992).
[40]C. Choi and R. Elber, J. Chem. Phys. **94**, 751 (1991).
[41]E. J. Corat and D. G. Goodwin, J. Appl. Phys. **74**, 2021 (1993).
[42]M. D. Perry and L. M. Raff, J. Phys. Chem. **98**, 4375 (1994).
[43]E. Kondoh, T. Ohta, T. Mitomo, and K. Ohtsuka, Appl. Phys. Lett. **59**, 488 (1991).
[44]T. Tsuno, T. Imai, Y. Nishibayashi, K. Hamada, and N. Fujimori, Jap. J. Appl. Phys. **30**, 1063 (1991).
[45]M. Frenklach, S. Skokov, and B. Weiner, Nature (London) **372**, 535 (1994).